

Stability of dark solitons in a Bose-Einstein condensate trapped in an optical lattice

P. G. Kevrekidis,¹ R. Carretero-González,² G. Theocharis,³ D. J. Frantzeskakis,³ and B. A. Malomed⁴

¹*Department of Mathematics and Statistics, University of Massachusetts, Amherst, Massachusetts 01003-4515, USA*

²*Nonlinear Dynamical Systems Group,* Department of Mathematics & Statistics, San Diego State University, San Diego, California 92182-7720, USA*

³*Department of Physics, University of Athens, Panepistimiopolis, Zografos, Athens 15784, Greece*

⁴*Department of Interdisciplinary Studies, Faculty of Engineering, Tel Aviv University, Tel Aviv 69978, Israel*

(Received 29 April 2003; published 19 September 2003)

We investigate the stability of dark solitons (DSs) in an effectively one-dimensional Bose-Einstein condensate in the presence of the magnetic parabolic trap and an optical lattice (OL). The analysis is based on both the full Gross-Pitaevskii equation and its tight-binding approximation counterpart (discrete nonlinear Schrödinger equation). We find that DSs are subject to weak instabilities with an onset of instability mainly governed by the period and amplitude of the OL. The instability, if present, sets in at large times and it is characterized by quasiperiodic oscillations of the DS about the minimum of the parabolic trap.

DOI: 10.1103/PhysRevA.68.035602

PACS number(s): 03.75.Lm, 52.35.Mw, 05.45.-a

The experimental creation and great advancement in the theoretical understanding of Bose-Einstein condensates (BECs) [1] have stimulated a lot of interest in nonlinear matter waves, including dark [2] and bright [3] solitons. The dynamics of dark solitons (DSs) in the presence of the external magnetic trap has been extensively studied [4], including thermal [5] and dynamical [6] instabilities. More recently, apart from the rectilinear DSs, ring-shaped counterparts were predicted in BECs [7].

The study of nonlinear excitations is particularly relevant for BECs trapped in optical lattices (OLs) generated by interference patterns from laser beams illuminating the condensate [8–13]. The controllable character of the OL allows for the observation of numerous phenomena, such as Bloch oscillations [10,14] and Zener tunneling [8] (in the presence of an additional linear external potential), or classical [15] and quantum [13] superfluid-insulator transitions.

Apart from the mean-field description via the Gross-Pitaevskii (GP) equation [8–13], a BEC trapped in a strong OL may be described, in the tight-binding limit, by the discrete nonlinear Schrödinger (DNLS) equation [16]. This approximation is not always accurate, but its applicability can be systematically examined [17,18]. In cases where such a reduction is possible (e.g., when the chemical potential is much lower than the height of the potential barriers induced by the OL), the DNLS model is particularly relevant and has been successfully applied in many instances (for a recent review on DNLS, see, e.g., Ref. [19] and references therein).

In this paper, we study DSs in repulsive BECs (i.e., positive-scattering-length collisions) in the presence of OLs. We use both the continuous-GP and DNLS equations. In particular, we assume a cigar-shaped BEC (transverse directions smaller than the healing length [1]), which can be described by the normalized quasi-one-dimensional GP equation [1,20,21]

$$i u_t = -u_{xx} + |u|^2 u + [kx^2 + V_0 \cos^2(2\pi x/\lambda)] u. \quad (1)$$

Here, $u(x,t)$ is the mean-field wave function, while the terms in the square brackets represent the external magnetic trap and the OL potential, respectively, with the strengths k and V_0 , while λ is the wavelength of the interference pattern created by the laser beams.

To study the dynamics of a DS in the framework of Eq. (1), we consider an initial condition similar to an ansatz proposed for the description of DSs in BECs in Ref. [22],

$$u_0(x) = u_{\text{TF}}(x) \tanh(x - x_0), \quad (2)$$

where $u_{\text{TF}} = \sqrt{\max(0, \mu - kx^2)}$ is the Thomas-Fermi (TF) expression for the background wave-function distribution [1] (μ is the chemical potential) and x_0 is the initial location of the DS's center. In most cases, we set $x_0 = 0$, i.e., the dark soliton is placed at the bottom of the magnetic trap. The choice for a TF background is motivated by the fact that it is a good approximation for the steady-state atomic density when $V_0 = 0$ [1].

In the tight-binding limit, Eq. (1) reduces to the following DNLS equation [16],

$$i \dot{u}_n = -C(u_{n+1} + u_{n-1} - 2u_n) + |u_n|^2 u_n + kn^2 u_n, \quad (3)$$

where the dot denotes time derivative, n is the lattice-site index, and C is the coupling constant (see, e.g., Refs. [16–18] for exact expressions and relevant estimates). An initial condition for a DS in the case of Eq. (3) can be given by a straightforward discretization of the continuum ansatz (2). Typically, simulations were run for a lattice with 200 sites, and free boundary conditions for both the continuum and discrete models. In fact, it has been verified that the results are insensitive to the choice of boundary conditions. Note that DSs in discrete lattices (in the absence of parabolic trap) were already studied in the framework of the DNLS equation [23], revealing that they are subject to oscillatory instabilities [24].

Stationary solutions to Eq. (3) are sought for in the form $u_n = \exp(-i\mu t)v_n$, where μ is the chemical potential [1], which leads to the steady-state equation

*<http://nlds.sdsu.edu/>

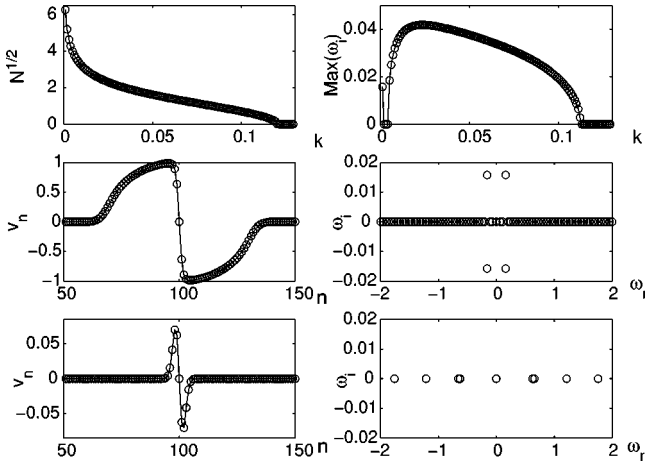


FIG. 1. The left and right top panels show, respectively, the (square root of the) number of atoms in the condensate N and the largest unstable eigenfrequency ω_i for the discrete dark soliton as a function of k for $C=1$. The profile of the (exact) solution is shown, for $k=0.001$ and $k=0.119$ (just prior to the termination of the branch), in the left middle and bottom panels, respectively. The right middle and bottom panels show the spectral plane (ω_r, ω_i) of the corresponding eigenfrequencies, the subscripts standing for the real and imaginary parts.

$$-C(v_{n+1} + v_{n-1} - 2v_n) + (|v_n|^2 + kn^2 - \mu)v_n = 0 \quad (4)$$

for a discrete function v_n . Once a solution of Eq. (4) is found, linear stability analysis is performed by looking for perturbed solutions of the form

$$u_n = e^{-i\mu t} [v_n + \epsilon a_n e^{i\omega t} + \epsilon b_n e^{-i\omega^* t}], \quad (5)$$

where the asterisk denotes complex conjugation. The ensuing eigenvalue problem, for the eigenfrequency-eigenfunction pair $\{\omega, \{a_n, b_n^*\}\}$, is then solved numerically with $\omega = \omega_r + i\omega_i$ (where the subscripts denote the real and imaginary parts). In what follows, since Eqs. (1) and (3) admit an additional rescaling, the chemical potential has been fixed at $\mu = 1$.

We first consider the DNLS model with a fixed coupling constant $C=1$ while the strength k of the parabolic trap is varied. In this case, it is found that the assumed configuration, in the form of a DS on top of the TF background, exists only up to a critical value of $k_{cr} \approx 0.12$, as is seen from the top left panel of Fig. 1, which complies with the well-known fact that the DS cannot have a width essentially smaller than the healing length [1], and thus cannot exist in a very narrow trap.

This solution family is quantified by the top panels of Fig. 1. The norm $N \equiv \|v_n\|_2^2 = \sum_n v_n^2$ (number of atoms N) as a function of k is depicted in the top left panel. The dependence of the largest instability growth rate ω_i on k , which is shown, for the same discrete-DS solution, in the top right panel of Fig. 1, reveals a narrow stability window close to $k=0$ (for $0.002 \leq k \leq 0.004$). At larger values of k , the DS is always subject to an oscillatory instability similar to that found for regular dark optical solitons [24]. Nevertheless,

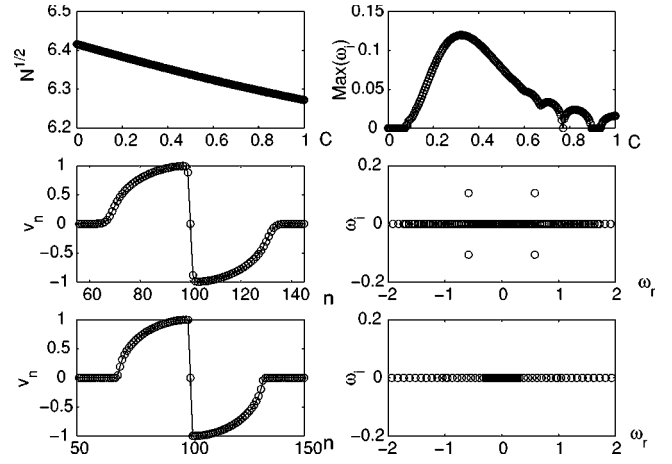


FIG. 2. The top panels in Fig. 2 are equivalent to those in Fig. 1, but now the strength of the trapping potential is fixed, $k=0.001$, while the coupling constant C is varied. The middle and bottom panels show, respectively, examples of the spatial profiles and eigenfrequency spectral planes of unstable (for $C=0.25$) and stable (for $C=0.01$) DSs.

this instability is characterized by a *small* growth rate, whose maximum value is $\omega_i \approx 0.04$ (at $k \approx 0.024$).

An example of the weakly unstable DS for $k=0.001$ can be seen in the middle panels of Fig. 1, and an example close to the termination of the branch (at $k=0.119$) is shown in the bottom panels. Note that the instability is manifested by the presence of a nonzero imaginary part of the eigenfrequencies.

Next, we consider the case where the strength of the parabolic trap is kept fixed, $k=0.001$, while the coupling constant C is varied in the interval $0 \leq C \leq 1$. In this case, the DS configuration on top of the TF background has been obtained for every value of C , see Fig. 2, down to $C=0$ corresponding to the so-called anticontinuum limit. The norm of the solution (top left panel of Fig. 2) is a slowly (almost linearly) decreasing function of C , which can be easily understood. Indeed, since the effective size of the TF distribution is kept constant (the trap strength k is fixed), the DS placed at the center of the condensate expands to a larger number of lattice sites as C increases, hence a bigger internal part of the BEC cloud is effectively devoid of atoms. The dependence of the largest unstable eigenfrequency ω_i on C , shown in the top right panel of Fig. 2, reveals that there exist a critical value $C_{cr} \approx 0.076$ at which a Hamiltonian-Hopf bifurcation occurs, as two pairs of eigenvalues with opposite *Krein signatures* [25] collide and bifurcate into a complex quartet.

Notice the proximity of the critical value observed herein and the one found in Ref. [24] for optical DSs (without the parabolic trap). This observation suggests that the presence of the parabolic trap does not significantly affect the threshold of the oscillatory instability.

It is noteworthy that, at larger values of C (see the top right panel of Fig. 2), there are windows on the C axis (e.g., $0.895 \leq C \leq 0.935$ for the 200-site lattice) where the DS is stable. Examples of unstable (for $C=0.25$) and stable DSs (for $C=0.01$), as well as the respective spectral planes (ω_r, ω_i) of the eigenfrequencies, are shown in the middle

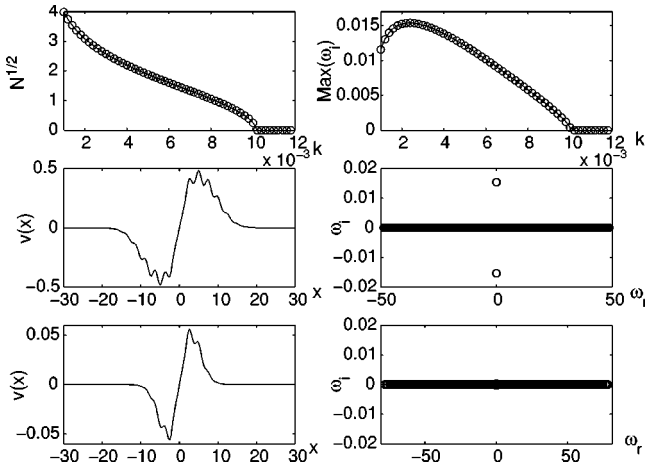


FIG. 3. The top panels show the number of atoms rescaled (for convenience) by a factor of $10^{-1/4}$ (left) and the maximum of the instability growth rate ω_i (right) for the dark soliton vs the parabolic trap strength k , as found from the continuum Gross-Pitaevskii equation (1) with $V_0=1.5$ and $\lambda=5$. The middle and bottom panels display the spatial profiles for the dark solitons with $k=0.024$ and $k=0.01$ (left) and the respective stability spectral planes (right). ($k=0.01$ being very close to the termination point of the branch.)

and bottom panels of Fig. 2. As noted in Ref. [24], the stability windows result from the finiteness of the lattice.

As the DNLS of Eq. (3) is only a tight-binding approximation of the full continuum model, i.e., the GP equation (1), it is necessary to investigate whether and how the weak instability of the DSs, demonstrated above in the discrete limiting case, manifests itself in the full GP equation. To this end, we first consider the case where the OL potential is fixed (an analog of the case where C is fixed in the discrete model), with strength $V_0=1.5$ and wavelength $\lambda=5$.

Similar to what we find for the discrete case, the DS on the TF background exists, in the continuum GP equation, only up to a critical value of the trap strength, $k_{cr} \approx 0.01$. This is demonstrated in the top left panel of Fig. 3, where the number of atoms, which is now defined as $N = \|v\|_2^2 \equiv \int_{-\infty}^{+\infty} |v(x)|^2 dx$, is shown versus k . Furthermore, the eigenvalue computation shows that this family of continuum DSs is always unstable (although in other cases DSs in the continuum model may be stable, see below). However, the instability is *extremely weak*, as its largest growth rate $\max(\omega_i) \approx 0.015$ (at $k \approx 0.024$). The shape of typical continuum DSs are shown in the middle and bottom panels of Fig. 3 together with the corresponding spectral planes.

Next, we consider the case where the strength of the magnetic trap, in the continuum GP equation, is fixed at $k=0.001$, while the wavelength λ of the OL is varied (the strength of the OL is again $V_0=1.5$). In this case, the DS on the TF background exists for every value of λ in an interval $3 \leq \lambda \leq 5$, which is chosen to display the present case. In particular, the top left panel in Fig. 4 shows the number of atoms in the DS as a function of λ . Furthermore, the dependence of the largest instability growth rate ω_i on λ (top right panel in Fig. 4) reveals that a Hamiltonian-Hopf bifurcation occurs at a critical point, $\lambda_{cr}^{(1)} \approx 4$, so that the DSs are stable

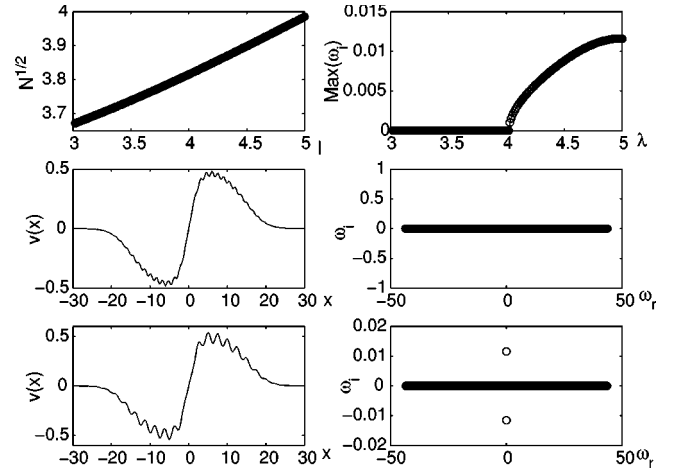


FIG. 4. The top panels show the number of atoms in the continuum dark soliton (rescaled by the factor $10^{-1/4}$, left) and the largest instability growth rate ω_i (right) vs the OL wavelength λ for the GP equation with $V_0=1.5$ and $k=0.001$. The middle and bottom panels show the spatial profile of the dark solitons for $\lambda=3$ and $\lambda=5$ (left) and their respective spectral planes (right).

for $\lambda < \lambda_{cr}^{(1)}$ and unstable otherwise. Examples of stable and unstable DSs for $\lambda=3$ and $\lambda=5$ are shown in the middle and bottom panels in Fig. 4, together with their respective spectral planes. We have verified that for $\lambda < 3$ the DS retains its stability, while for $\lambda > 5$ it remains unstable up to $\lambda < \lambda_{cr}^{(2)} \approx 5.45$ and restabilizes for larger values of λ . After running simulations at many other parameter values, we have concluded that the OL periodicity λ is a crucial factor in determining the stability of the DS in the continuum GP equation, while the strength of the parabolic trap k plays a lesser role.

Finally, an additional factor of relevance in determining stability is the amplitude V_0 of the optical lattice. We have found (data not shown) that variation of V_0 results in the presence of windows of stability for a fixed value of λ . For instance, for $\lambda=5$, the soliton is stable in the absence of the optical lattice (i.e., for $V_0=0$) as well as, e.g., in the intervals $V_0 \in [0.04, 0.13]$ or $V_0 \in [1.17, 1.38]$, while it is unstable for intermediate values.

In the case where solitons are unstable, it is desirable to directly simulate the full nonlinear equation, in order to observe the evolution of the soliton under the effect of the instability. We find that the instability sets in at large times, on the order of $O(100)$, and manifests itself as follows: the DS, which is initially placed at the bottom of the composite potential (magnetic trap and OL), performs small-amplitude oscillations inside the respective small well of the OL potential. Then, as time passes, the soliton starts to emit small amounts of radiation, and as a result, it gains enough kinetic energy to perform larger-amplitude quasiperiodic oscillations around the center of the condensate. This behavior is demonstrated in the left panel of Fig. 5, where two snapshots of the density profile of the DS are shown at $t=0$ and $t=700$ for the unstable DS of the bottom panel of Fig. 4. To trigger the onset of instability, a uniformly distributed random per-

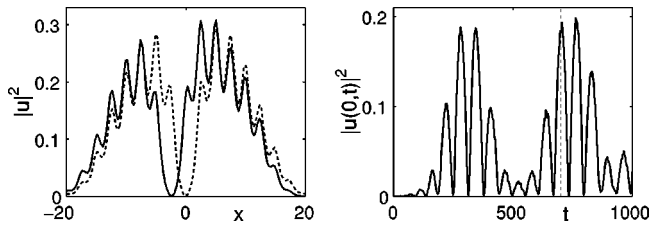


FIG. 5. Left: the profile of the dark soliton at $t=0$ (dashed line) and $t=700$ (solid line). Right: time evolution of the density, $|u(x,t)|^2$, at the central point $x=0$. $V_0=1.5$, $\lambda=5$, and $k=0.001$.

turbation of amplitude 0.01 is added to the initial configuration. It can be clearly observed that, in the final state, the DS has shifted its position from the center of the condensate ($x=0$). Quasiperiodic oscillations of the density at the point $x=0$, induced by the instability, are shown in the right panel of Fig. 5.

In conclusion, we investigate the existence and stability of stationary DSs in repulsive BECs, trapped in an OL. The consideration is performed in the framework of both the con-

tinuous GP equation and its discrete tight-binding dynamical-lattice counterpart, taking into regard the effect of the external magnetic trap and OL. We find that in the discrete model the DSs are, generally, subject to a *weak* oscillatory instability. In the full GP equation, DSs may be stable and the stability is chiefly determined by the period and amplitude of the OL. If the oscillatory instability is present, it sets in at large times, which attests to the robustness of DSs. The instability eventually manifests itself as a shift of the DS from the center of the condensate, which is accompanied by quasiperiodic oscillations. This work can be naturally extended for two-dimensional vortices. First steps in that direction were made in Refs. [26] and [27].

This work was supported by a UMass FRG and NSF-DMS-0204585 (P.G.K.), the Special Research Account of the University of Athens (G.T., D.J.F.), the Binational (US-Israel) Science Foundation (Grant No. 1999459), the San Diego State University Foundation (R.C.G.), and a Windows-on-Science grant from the European Office of Aerospace Research and Development of the US Air Force (B.A.M.).

-
- [1] F. Dalfovo *et al.*, Rev. Mod. Phys. **71**, 463 (1999).
 [2] S. Burger *et al.*, Phys. Rev. Lett. **83**, 5198 (1999); J. Denschlag *et al.*, Science **287**, 97 (2000); B.P. Anderson *et al.*, Phys. Rev. Lett. **86**, 2926 (2001).
 [3] K.E. Strecker *et al.*, Nature (London) **417**, 150 (2002); L. Khaykovich *et al.*, Science **296**, 1290 (2002).
 [4] W.P. Reinhardt and C.W. Clark, J. Phys. B **30**, L785 (1997); Th. Busch and J.R. Anglin, Phys. Rev. Lett. **84**, 2298 (2000); D.J. Frantzeskakis *et al.*, Phys. Rev. A **66**, 053608 (2002).
 [5] P.O. Fedichev *et al.*, Phys. Rev. A **60**, 3220 (1999); A. Muryshv *et al.*, Phys. Rev. Lett. **89**, 110401 (2002).
 [6] D.L. Feder *et al.*, Phys. Rev. A **62**, 053606 (2000); J. Brand and W.P. Reinhardt, *ibid.* **65**, 043612 (2002).
 [7] G. Theocharis *et al.*, Phys. Rev. Lett. **90**, 120403 (2003).
 [8] B.P. Anderson and M.A. Kasevich, Science **282**, 1686 (1998).
 [9] C. Orzel *et al.*, Science **291**, 2386 (2001).
 [10] O. Morsch *et al.*, Phys. Rev. Lett. **87**, 140402 (2001).
 [11] F.S. Cataliotti *et al.*, Science **293**, 843 (2001).
 [12] M. Greiner *et al.*, Phys. Rev. Lett. **87**, 160405 (2001).
 [13] M. Greiner *et al.*, Nature (London) **415**, 39 (2002).
 [14] D.I. Choi and Q. Niu, Phys. Rev. Lett. **82**, 2022 (1999).
 [15] F.S. Cataliotti *et al.*, New J. Phys. **5**, 71 (2003); A. Smerzi *et al.*, Phys. Rev. Lett. **89**, 170402 (2002).
 [16] A. Trombettoni and A. Smerzi, Phys. Rev. Lett. **86**, 2353 (2001); F.K. Abdullaev *et al.*, Phys. Rev. A **64**, 043606 (2001).
 [17] G.L. Alfimov *et al.*, Phys. Rev. E **66**, 046608 (2002).
 [18] N.K. Efremidis and D.N. Christodoulides, Phys. Rev. A **67**, 063608 (2003).
 [19] P.G. Kevrekidis *et al.*, Int. J. Mod. Phys. B **15**, 2833 (2001).
 [20] P.A. Ruprecht *et al.*, Phys. Rev. A **51**, 4704 (1995).
 [21] V.M. Pérez-García *et al.*, Phys. Rev. A **57**, 3837 (1998); L. Salasnich *et al.*, *ibid.* **65**, 043614 (2002); Y.B. Band *et al.*, *ibid.* **67**, 023602 (2003).
 [22] R. D'Agosta *et al.*, Phys. Lett. A **275**, 424 (2000).
 [23] Yu.S. Kivshar *et al.*, Phys. Rev. E **50**, 5020 (1994).
 [24] M. Johansson and Yu.S. Kivshar, Phys. Rev. Lett. **82**, 85 (1999).
 [25] J.-C. van der Meer, Nonlinearity **3**, 1041 (1990).
 [26] P.G. Kevrekidis *et al.*, J. Phys. B **36**, 3467 (2003).
 [27] B.B. Baizakov *et al.*, Europhys. Lett. **63**, 642 (2003).